

AUTOMATED BROAD AREA CALIBRATION FOR CODA BASED MAGNITUDE AND YIELD

W. Scott Phillips, Howard J. Patton, Claudia M. Aprea, Hans E. Hartse, George E. Randall and Steven R. Taylor

Los Alamos National Laboratory

Sponsored by National Nuclear Security Administration
Office of Nonproliferation Research and Engineering
Office of Defense Nuclear Nonproliferation

Contract No. W-7405-ENG-36

ABSTRACT

The stability of local (< 100 km) earthquake coda has been well established through observations that have shown coda amplitudes to be independent of distance, path details and azimuth with respect to the focal mechanism. This behavior is consistent with scattered energy models of coda and allows accurate measurement of relative amplitudes for use in source scaling or site effect studies. Furthermore, coda amplitudes can be measured to high precision because of the redundant information in adjacent time windows. Mayeda (2003) has recently extended coda wave techniques to regional distances, through the empirical calibration of distance-dependent coda shape. Using this technique, we apply coda analysis to a regional network (38 sites) covering China and central Asia. The analysis of large amounts of data is accomplished using automatic techniques to isolate coda, calibrate coda shape, obtain and apply path, site and coda generation corrections and shift to absolute level. The path and site corrections are obtained using amplitude difference tomography, which eliminates source terms from the inversion. For 13 bands between 0.03 and 8 Hz and datasets of up to 2250 multiple recorded events, residuals (RMS) are reduced to less than 0.1 log₁₀ amplitude units. For 0.7 to 1 Hz data, variance reduction is 86% relative to the best fit uniform attenuation model. The resulting attenuation patterns closely follow regional geology. After calibration, we can directly compare scaling behavior of explosions across the region, which includes the Semipalatinsk and Lop Nor test sites. Ties can be made to parameters of monitoring interest, such as m_b . We can also directly compare spectra from a wide distribution of earthquakes, showing regional variations in source scaling that should be incorporated into event identification and coda calibration procedures.

OBJECTIVE

We calibrate coda wave behavior, including site and path effects, in order to isolate and study source phenomena and to determine magnitude and yield. Our objective is to develop a transportable methodology that can be used to characterize events to a small size threshold over broad areas. Because manual review of coda envelopes requires substantial time investment, we develop methods to process the data in an automated manner.

RESEARCH ACCOMPLISHED

The stability of coda waves has been well established through observations that have shown coda amplitudes to be independent of distance, path details and azimuth with respect to the focal mechanism (Aki, 1969). This behavior is consistent with the generation of coda by scattering and allows accurate measurement of relative amplitudes for use in source scaling (e.g. Aki and Chouet, 1975) or site effect (Phillips and Aki, 1986) studies. Furthermore, coda amplitudes can be measured to high precision because of the redundant information in adjacent time windows. This makes coda ideal for monitoring small, sparsely recorded events for purposes of discrimination (Hartse et al., 1995) and magnitude or yield estimation (Rautian et al., 1979; Mayeda, 1993) as the measurement stability is equivalent to that available from a multi-station network.

We apply the regional coda calibration methods developed by Mayeda et al. (2003) to obtain coda calibration parameters for China and central Asia stations. We processed 13,315 records from 157 nuclear tests, 28 chemical explosions and 5914 earthquakes recorded at 38 sites (Figure 1) for purposes of calibrating China and central Asia coda wave behavior. Including duplicate and surrogate stations in the list, these are: AAK, BJI, BJT, BRV, BRVK, CHTO, ENH, HIA, KMI, KKAR, KK31 KUR, KURK, LSA, LZH, MAK, MAKZ, MKAR, MK31, MDJ, NIL, NVS, PDY, QIZ, SSE, TKM2, TLG, TLY, ULHL, ULN, WMQ, WUS, XAN and ZAL, as well as Borovoye archive STsR-TSG instruments KS, KSM and KSVM (Richards et al., 1992; Kim and Ekstrom, 1996) and PASSCAL Tibetan Plateau Experiment stations AMDO, BUDO, ERDO, GANZ, LHSA, MAQI, SANG, TUNL, USHU, WNDO and XIGA (Owen et al., 1993).

Following instrument correction, data were reduced by band-passing in 13 bands, from 0.03-0.05 to 6.0-8.0 Hz, followed by Hilbert transform envelope and smoothing operations. Final envelopes were formed by averaging the two horizontal component envelopes. Exceptions are the vertical components at short-period arrays and Borovoye archive KSVM. MKAR and KKAR array envelopes were stacked without shifting, which reduced the scatter that typically rides on top of the envelope, allowing better detection of low signal-to-noise coda, especially in the higher frequency bands.

Coda analysis windows were determined by manual inspection for a subset of the China and central Asia envelope data that included all BRV(K), KKAR, MAK(Z), MKAR, NIL (BH), ULN, WMQ and Tibet Experiment records, all explosions, both nuclear and chemical, as well as all records of 44 earthquakes for which independently derived moments exist. The remaining data were analyzed using an automatic procedure to identify the coda window. This procedure was designed to stop short of secondary events or noise sources that can be present in the coda, as well as to extend the coda beyond poor, high estimates of noise level in cases where seismograms were triggered and little noise was available for measurement. Specifically, the method uses the expected coda shape to find the minimum amplitude point in the coda, and to project beyond that point until the envelope deviates too much from the model.

After manual review, we calibrated coda peak and shape parameters following the regional calibration procedure of Mayeda et al. (2003). First, we determined coda peaks by inspection of WMQ and NIL (BH) envelope data. In many cases, especially for low Q paths and high frequencies, peaks did not stand out; however a break in slope could be identified near the predicted Lg arrival. In some low Q path cases, the peak envelope occurred near the Sn arrival and no peak or break in slope could be identified near the Lg. Sn peaks were more commonly observed at NIL than at WMQ. Sn coda were used in the analysis if signal-to-noise were sufficient following the predicted Lg peak. The group velocities of the envelope peaks were calibrated by fitting (L_1) a flat Lg velocity along with a hyperbola with three adjustable parameters to describe the Sn velocity as a function of distance:

$$v_g = v_0 - \frac{v_1}{v_2 + \Delta}$$

where v_g is group velocity of the peak; v_0 , v_1 and v_2 are adjustable parameters and Δ is distance in kilometers. Within scatter, Sn and Lg group velocities were the same for WMQ and NIL, so we applied these calibration curves to all stations.

Coda shape was obtained by fitting the coda decay using:

$$a(t) = a_0 \cdot t^{-\alpha} \cdot e^{\beta \cdot t}$$

where $a(t)$ is coda amplitude, t is time from the coda peak (taken as the smaller of the Lg and Sn velocities, see above), a_0 is the coda source factor, α is a spreading factor, set to 0.7 for all data and β is the coda decay parameter. The decay parameter was then calibrated as a function of distance by varying hyperbola parameters b_0 , b_1 and b_2 to best fit (L_1) the coda envelope data:

$$\beta = b_0 - \frac{b_1}{b_2 + \Delta}$$

The coda shape parameters were determined for various station groups. Well sampled stations, such as WMQ, were calibrated alone. Closely located stations, such as MAK, MAKZ, MKAR and MK31, or Kirgiz network stations, were grouped together. Poorly sampled stations were grouped by regional propagation characteristics (based on 2D amplitude tomography results, described below).

Using the calibrated envelope peak group velocity and coda shape factor, we obtain raw coda source factors, a_0 above, by fitting using the coda decay formula. These values must be corrected for path and site effects. We use 1D and 2D methods to do this. The 1D method follows Mayeda et al. (2003). We start with a rough source correction based on m_b (Taylor and Hartse, 1998) and fit (L_1) a spreading-attenuation model:

$$a(\Delta) = s_0 \cdot \Delta^{-\alpha} \cdot e^{\frac{-\pi f \Delta}{Qc}}$$

where a is m_b -corrected amplitude, s_0 represents the site effect, but contains other effects such as coda generation (media scattering strength), α is spreading, f is frequency, Q is the quality factor and v is velocity, to which we assign the nominal Lg velocity of 3.5 km/s. Spreading is set based on m_b -corrected coda amplitudes at distances under 100 km. These values are zero at low frequencies and increase (0.7 for the 6 - 8 Hz band) with frequency. These values reflect the shrinking range over which coda amplitude is observed to be independent of distance as frequency increases. Site and Q terms are varied to obtain the best fit. While appearing physical, this equation is only used for empirical fitting and fit parameters must not be overinterpreted. These site and Q values are used as the starting point for a second refinement step.

The site and Q terms are further refined using data only from events recorded at more than one station. This is done by adjusting the site and Q models simultaneously for all stations in order to fit station-to-station amplitude ratios. This removes the influence of a possibly biased m_b , which was used in the initial step to remove source effects (Mayeda et al., 2003). We implement this procedure using an L_1 criterion with direct search techniques (Press et al., 2001). We note that the heterogeneous seismicity pattern results in sampling over limited distance ranges for many stations, which makes extrapolation risky using the 1D results.

Our preferred path correction method employs tomography techniques to invert for a laterally varying (2D) Q and relative site terms (Phillips et al., 2000; Phillips et al., 2001; Phillips and Hartse, 2002). The inversion equations are the same as for the 1D case, above, with the addition of a sum over discretized path terms in place of $1/Q$. We only use data from multiply recorded events, similar to the second, 1D path step, in order to eliminate source effects by fitting station-to-station amplitude ratios. We remove a small number of outliers (less than 1% of the data) based on the 1D results and use L_2 techniques in the inversion. Spreading is set as in the 1D calculations. Currently, the tomography treats the coda as a direct path, rather than an ellipsoidal area. This is most appropriate for short codas; however, misfits are low as RMS residuals fall below 0.1 log10 amplitude units for all bands. For data from 2250 multiply recorded events in the band 0.7 to 1 Hz, for example, residual variance is reduced 86% relative to the best

fit, uniform Q model. Q results follow regional geology well. We are confident in our ability to extrapolate path corrections into aseismic areas because of the more physical nature of the tomography model.

The final calibration steps adjust measurements between bands and shift to absolute units based on independently determined moments. Adjustments between bands are calculated in order to flatten earthquake spectra below their corners. Corner frequencies are estimated using scaling based on m_b (Taylor and Hartse, 1998). We start with earthquake data from bands less than 1/4 of the corner frequency in an L_1 simplex inversion to obtain the band corrections. For our dataset, this gives corrections for bands below 1 Hz. We assume an ω^2 model and allow data less than 1/2 the corner, and so on, to obtain corrections for the higher bands, which are spliced to the low frequency results. This approach was suggested by results of synthetic tests that showed that high frequency spectra can drift high by 0.1 to 0.2 \log_{10} units, likely due to a slight curvature of earthquake spectra when using a liberal corner frequency cutoff.

We are fortunate to have data from 44 earthquakes for which moments have been independently determined using waveform matching techniques (Zhu et al., 1997; Patton, 1998; Ghose et al., 1998). An overall shift is obtained such that spectral data from bands less than 1/4 of the corner frequency, calculated as above, match the appropriate moment in a median sense. Spectra then carry units of N-m. Earthquake results become moment rate spectra and we refer to explosion results as apparent coda source spectra, the term apparent indicating possible near source effects, including near source path, on the spectra.

After correction, the scatter between coda and independently derived moments is 0.18 \log_{10} units. We do not use CMT solutions in this step because of bias due to unaccounted for crustal thickness in this area (Patton, 1998). Additional independent moments will be needed in the future to further validate our results. A broad geographical distribution would help validate the broad area calibration. Moments for small events, perhaps obtained by applying spectral techniques to local network data, would help validate the results in higher bands.

Apparent source spectra for a well recorded Lop Nor nuclear event show good correspondence between stations (Figure 2). These spectra match especially well in the higher bands. Low frequency coda are less well studied, but are known to exhibit multipathing effects (Patton et al., 1985). Spectra from a suite of Degelen explosions show a marked scaling of the spectral peak (Figure 3). These spectral peaks occur in higher bands than has been observed for NTS explosions (Mayeda and Walter, 1996) and may reflect more competent emplacement material.

The earthquake results can be summarized by fitting a two-parameter ω^2 source model. We then calculate M_w and stress drop using standard formulae. Stress drop for network spectral fits show striking regional variation in China and central Asia (Figure 4). The patterns include low stress drop events (0.1 MPa) in areas of north-central Tibet and the North China Basin. A marked gradient in stress drop can be seen starting at the Tarim Basin-Tien Shan boundary where stress drops are uniformly about 1 MPa, then moving north into the Tien Shan where stress drops increase to above 10 MPa and finally approach 100 MPa. The stress drop patterns tend to be similar from station to station. Furthermore, for station WMQ and others, the low stress Tibet events lie along similar paths as more distant, higher stress events. This indicates unaccounted for path effects are not the cause of the variations. Such variations in scaling should be included in amplitude calibration efforts for both event identification and characterization work.

CONCLUSIONS AND RECOMMENDATIONS

Broad area calibration using tomographic imaging for path and site effects allows coda spectra to be displayed on a common basis throughout China and central Asia, for both earthquakes and explosions. Residuals from the tomographic inversions are remarkably low, on the order of 0.1 \log_{10} units, demonstrating the internal consistency and precision of the amplitude data. Similar, two-dimensional patterns should be investigated in other coda calibration steps, including the group velocity of the peak envelope and coda shape effects.

The calibration steps are tied together by a single master script. This allows easy updating of results when methods are modified or new data or manual picks are added. This also allows synthetic tests to be run with minimal effort, which have given us insight into weaker links and generated upgrades in the calibration procedures. The critical

pieces of the automatic scheme are codes that determine the coda window, which have been designed to avoid secondary events and noise once the coda shapes are calibrated. Calibration is further aided by using robust, L_1 , inversion methods wherever possible and by bootstrapping from starting models based on manually picked data.

The coda results show interesting scaling for both explosion and earthquake sources. Explosion spectra peak in bands higher than has been found for NTS, which may have implications for transportability of event identification and characterization techniques. Earthquakes also show systematic, regional variations in scaling through stress drop patterns, which could be included in event identification work (MDAC) to reduce scatter in earthquake populations of discriminants, as well as in the coda procedures, where emphasis on high stress drop events would be useful in obtaining spectral flattening corrections.

REFERENCES

- Aki, K. (1969). Analysis of the seismic coda of local earthquakes as scattered waves, *J. Geophys. Res.*, 74, 615-631.
- Aki, K. and B. Chouet (1975). Origin of coda waves: attenuation, and scattering effects. *J. Geophys. Res.* 80, 3322-3342.
- Ghose, S., M.W. Hamburger and C.J. Ammon (1998). Source parameters of moderate sized earthquakes in the Tien Shan, central Asia from regional moment tensor inversion, *Geophys. Res. Lett.*, 25, 3181-3184.
- Hartse, H.E., W.S. Phillips, M.C. Fehler and L.S. House (1995). Single-station spectral discrimination using coda waves, *Bull. Seism. Soc. Am.*, 85, 1464-1474.
- Kim, W-Y. and G. Ekstrom (1996). Instruments responses of digital seismographs at Borovoye, Kazakhstan, by inversion of transient calibration pulses. *Bull. Seism. Soc. Am.* 86, 191-203.
- Mayeda, K.M. (1993). mb (Lg Coda): A stable single station estimator of magnitude, *Bull. Seism. Soc. Am.*, 83, 851-861.
- Mayeda, K.M., W.R. Walter (1996). Moment, energy, stress drop and source spectra of western United States earthquakes from regional coda envelopes, *J. Geophys. Res.*, 101, 11195-11208.
- Mayeda, K.M., A. Hofstetter, J.L. O Boyle, W.R. Walter (2003). Stable and transportable regional magnitudes based on coda-derived moment-rate spectra, *Bull. Seism. Soc. Am.*, 93, 224-239.
- Owens, T.J., G.E. Randall, F.T. Wu and R. Zeng (1993). PASCALL instrument performance during the Tibetan Plateau Passive Seismic Experiment, *Bull. Seism. Soc. Am.*, 83, 1959-1970.
- Patton, H.J., S.R. Taylor, D.B. Harris and J.M. Mills (1985). The utility of regional Chinese seismograms for source and path studies in central Asia, *Geophys. J. Royal Astr. Soc.*, 81, 469-478.
- Patton, H.J. (1998). Bias in the centroid moment tensor for central Asian earthquakes: Evidence from regional surface wave data, *J. Geophys. Res.*, 103, 26963-26974.
- Phillips, W.S. and K. Aki (1986). Site amplification of coda waves from local earthquakes in central California, *Bull. Seism. Soc. Am.*, 76, 627-648.
- Phillips, W.S., H.E. Hartse, S.R. Taylor and G.E. Randall (2000). 1 Hz Lg Q tomography in central Asia, *Geophys. Res. Lett.*, 27, 3425-3428.
- Phillips, W.S., H.E. Hartse, S.R. Taylor, A.A. Velasco and G.E. Randall (2001). Application of regional phase amplitude tomography to seismic verification, *Pure Appl. Geophys.*, 158, 1189-1206.

Phillips, W.S. and H.E. Hartse (2002). Regional path calibration using multiple station amplitude tomography, *Seism. Res. Lett.*, 73, 228.

Press, W.H., S.A. Teukolsky, W.T. Vetterling and B.P. Flannery (2001). *Numerical Recipes in Fortran 77: The Art of Scientific Computing*, Cambridge University Press, Cambridge, U.K.

Rautian, T.G., V.I. Khalturin, I.S. Shengelia, (1979). The coda envelopes and the determination of the magnitudes of Caucasus earthquakes, *The Physics of the Earth*, Acad. Sci. USSR, N6 22-29 (English translation of Russian original).

Richards, P.G., W.Y. Kim and G. Ekstrom (1992). The Borovoye Geophysical Observatory, Kazakhstan, *EOS*, 73, 201-206.

Taylor, S.R. and H.E. Hartse (1998). A procedure for estimation of source and propagation amplitude corrections for regional seismic discriminants, *J. Geophys. Res.*, 103, 2781-2789.

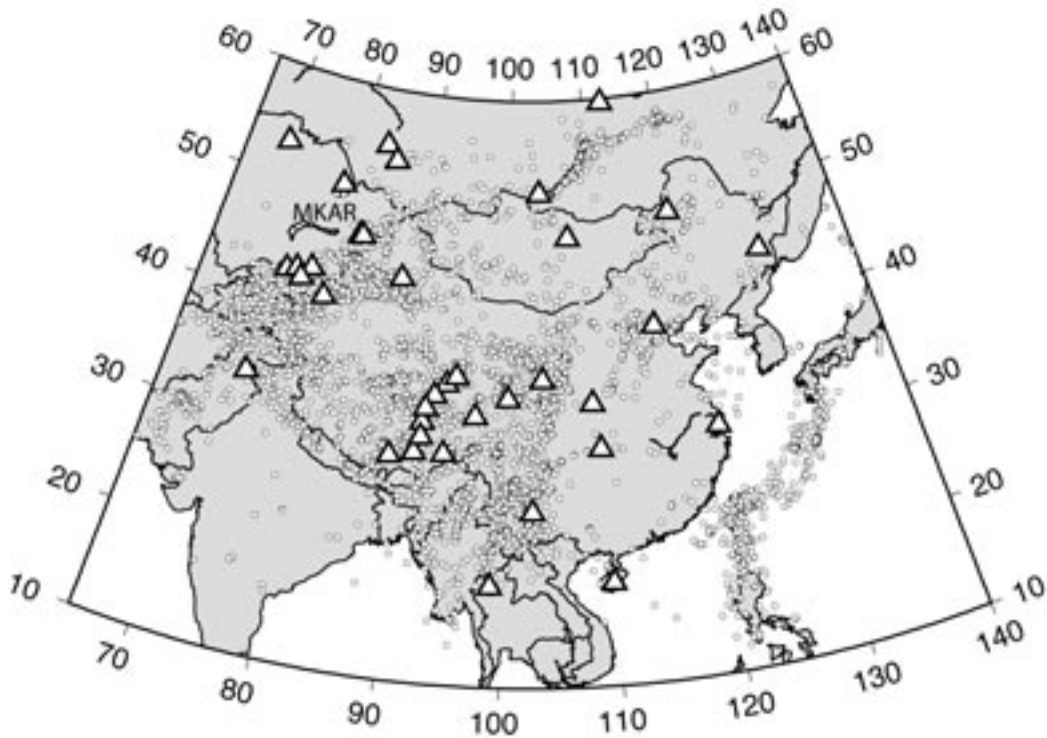


Figure 1. Stations and events used in the coda wave study.

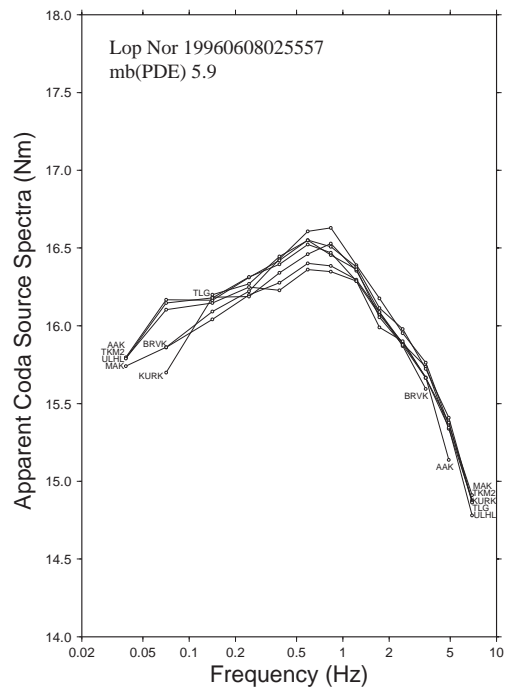


Figure 2. Apparent source spectra determined using coda wave data from seven stations for a Lop Nor test. Stations are indicated as spectra endpoints. The inter-station consistency is especially good for bands above 1 Hz.

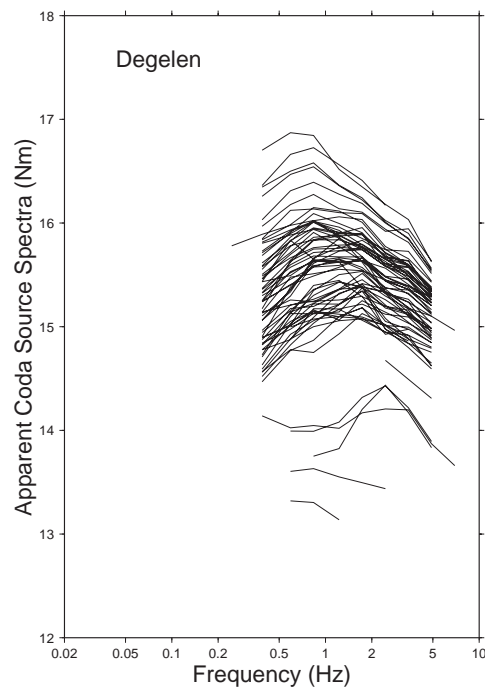


Figure 3. Apparent source spectra from coda for Degelen Mountain events, including the Omega series, 100 T chemical explosions.

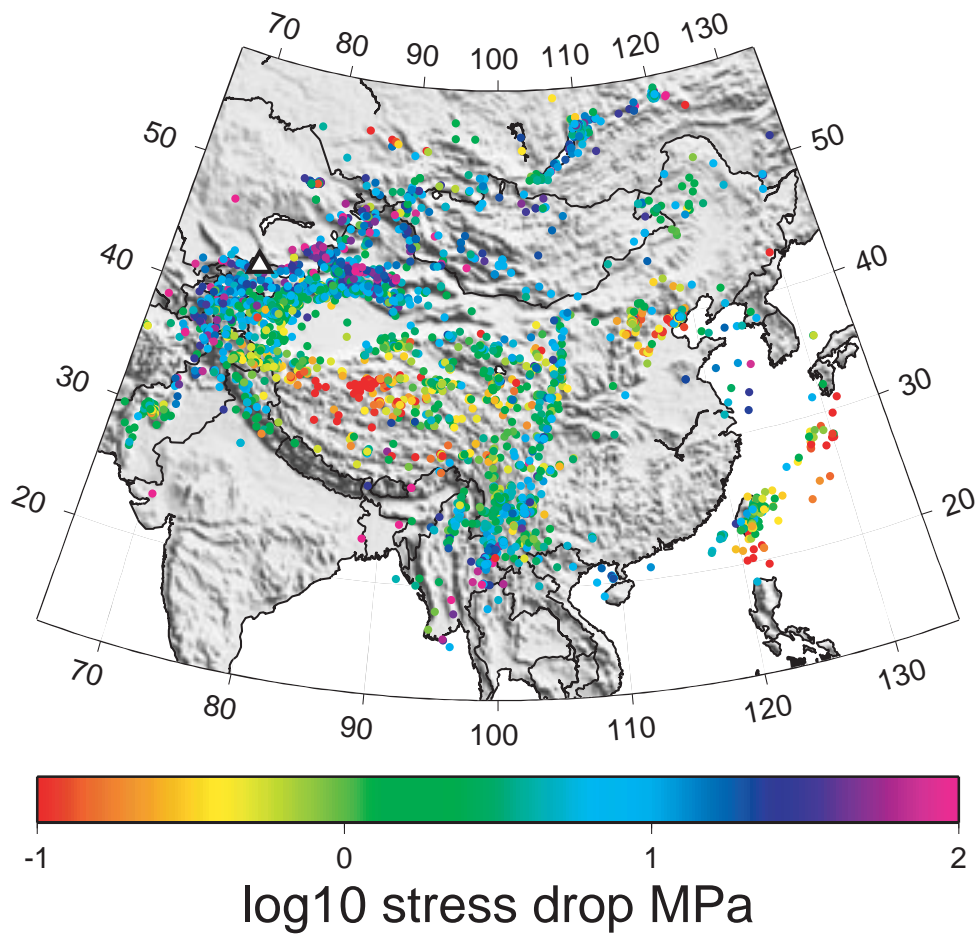


Figure 4. Network stress drop from coda spectra based on standard formulae.